Wave interaction with nonlinear damage and generation of harmonics in composite structures

R.K. Apalowo[a], D. Chronopoulos[a], S. Cantero-Chinchilla[a,b]

[a]*Institute for Aerospace Technology & The Composites Research Group, The University of Nottingham, NG7 2RD, UK*

[b]*Aernnova Engineering Division S.A., Madrid, 28034, Spain*

Abstract

Nonlinear inspection techniques are increasingly gaining more attention due to their high sensitivity to very small sizes of localised structural damage. This work thereby presents a generic Finite Element (FE) based computational scheme for quantifying guided wave interaction with Localised Nonlinear Structural Damage (LNSD) within structures of arbitrary layering and geometric complexity. The guided wave mode-shapes through the structure's thickness are initially computed through a Wave Finite Element (WFE) method. The scheme then independently applies the WFE obtained wave-mode of a specific wave type in a time domain FE simulation in order to define time harmonic excitations with appropriate amplitude. This generates a specific guided mode that propagates and interact with the LNSD and able to compute the generation of harmonics of the wave through an element activation and deactivation iteration. Numerical case studies are exhibited for the presented scheme. The scheme is validated against experimental measurements and a WFE-FE methodology for guided wave interaction with damage. Case studies for guided wave interaction with crack and delamination are also presented to study the dependence of the computed wave interaction coefficients on the severity of the LNSDs, and exhibit the capability of the presented scheme in classifying and identifying damage mode.

Keywords: Composite Structures, Nonlinear Ultrasound, Wave Interaction with Nonlinear Damage, Wave Finite Element Method, Finite Element Modelling.

Email address: eaxrka@nottingham.ac.uk (R.K. Apalowo)

Nomenclature

$\alpha, \beta, \alpha_0, \beta_0$	Nonlinear coefficients
$\mathbf{D}^*$	Condensed dynamic stiffness matrix
$\mathbf{K}, \mathbf{M}, \mathbf{D}$	Stiffness, mass and dynamic stiffness matrices of a modelled periodic segment
$\mathbf{T}$	Wave propagation transfer matrix
$\boldsymbol{\phi}, \boldsymbol{\Phi}$	Eigenvector and grouped eigenvector of the wave propagation eigenproblem
$\boldsymbol{K}_u^e$	Updated stiffness matrix of the elements in the damage zone
$\boldsymbol{q}$	Physical displacement vector for an elastic waveguide
λ	Propagation constant and eigenvector of the wave propagation eigenproblem
λ_{min}	Shortest wavelength within the bandwidth of the signal
O	Big O notation for nonlinear terms approximation
μ	Stiffness reduction factor
ω	Fundamental input angular frequency
$\Re$	Real operator
$\mathbf{f}$	Forcing vector for an elastic waveguide
Υ, u, χ	Output, input and scale factor of a dynamic system
ε_b	Strain between edges of damage front
ε_{dn}	Averaged nodal strain of each element in the damage zone
ε_d	Cumulative nodal strain of elements within the damage zone

A, B	Expansion coefficients
E, σ, ε	Elastic modulus, stress and strain of the medium
f_{max}	Highest frequency of interest
k	Wavenumber
L, R, I	Left, right sides and interior indices
l_e	Spatial FE discretization element size
L_x	Length of a waveguide's modelled periodic segment
N	Number of elements in the damage zone
p, P	Node index and total number of nodes along the lateral axis of the WFE modelled segment
q, f	Displacement and forcing indices
q_1, q_2	Nodal displacements of damage front edges
r	Periodic segment positioning index
t	Time
t_s	Integration time step of the FE transient analysis
w, W	Wave eigenvector index and total number of waves accounted for in the waveguide
x, y	In-plane and out-of-plane displacement indices

Contents

1 Introduction **4**

2 Wave interaction with localised nonlinear structural damage **8**

2.1 Wave constants calculation by a wave FE method 8

2.2 Localised nonlinear structural damage modelling 10

2.2.1 Harmonics generation through contact acoustic nonlinearity 10

2.2.2 Element birth/death criterion 11

2.3 Finite element wave interaction modelling 14

3 Case studies **15**

3.1 Experimental validation 15

3.2 Numerical case studies 17

3.2.1 Description and boundary condition of the model 18

3.2.2 Pristine plate 19

3.2.3 Interaction with crack 19

3.2.4 Interaction with delamination 22

4 Concluding remarks **25**

5 Data availability **27**

1. Introduction

The increased usage of composites structures in the aerospace and automotive industries has generally made non-destructive evaluation (NDE) of the structures not only more important but more demanding as well. This is because they exhibit a variety of failure modes, such as delamination, fibre breakage, matrix cracking and debonding, which must be frequently inspected in order to ensure continuous structural integrity. Ultrasonic NDE techniques are based on measuring certain wave properties, such as wave attenuation, frequency response, and interaction reflection or

transmission coefficients, in order to monitor and detect presence of damage in structural waveguides. Linear ultrasonic wave techniques have been widely developed for monitoring the condition and residual life estimation of in-service composite structures. However, these techniques are generally limited to relatively large defects but much less sensitive to micro and nonlinear defects. Therefore there is a need to develop nonlinear acousto-ultrasonic technique which will detect and evaluate nonlinear incipient defects in composite structures efficiently and reliably.

As early as [1], wave distortion and generation of higher harmonics during wave propagation in nonlinear medium have been considered. A numerical model for wave interaction with nonlinear coupling was first presented in [2, 3]. Harmonic generation in nonlinear wave interaction has hence been widely deployed for detecting contact-type defects (such as breathing cracks) as well as distributed deterioration (e.g. fatigue) in structural waveguides [4–11]. The developed models have been based on measuring the nonlinear wave effects which are pronounced in damaged and degraded structures but nearly incipient in the undamaged structures. Nonlinear elastic waves have also been widely applied to detect the presence of micro sized defects in composite structures. Wave propagation and material deterioration detection was investigated in 1D [12] and 2D [13] through a spring model. Numerical modelling of nonlinear wave interaction with an interface of rough surfaces in contact was studied in [14]. An alternative approach to nonlinear ultrasonic techniques was presented in [15] to investigate the non-collinear mixing of bulk shear waves for the purpose of measuring and eliminating nonlinearities in the system. Rayleigh waves were used in [16] to detect surface cracks and nonlinear longitudinal waves in [17] to evaluate closed cracks. An analytical scheme for modelling multi-modal wave interaction with damage was presented in [18, 19]. Reflection of compression and Rayleigh waves when impinging at the edge of an elastic plate was studied numerically in [20]. A coupled linear and nonlinear FE approach was developed in [21] to investigate wave interaction with damage in solid media. Recently, fatigue damage detection in composite structures using the higher harmonic generation was reported in [22]. A pitch-catch FE based approach was developed in [19, 23] to investigate nonlinearity introduced by breathing cracks. Inclusive reviews on the general progress of nonlinear wave interaction with damage and nonlinearities in structural media are presented in [24–27]. Despite the reported attempts to capture wave interaction with localised structural nonlinearities and damage, there

is currently no computational scheme for predicting these quantities for composite structures of arbitrary layering and geometric complexity.

Phased-array monitoring for enhanced life assessment (PAMELA) SHM system is one of the state-of-the-art SHM ultrasound system developed by Aernnova [28–30]. PAMELA is capable of generating signals up to 40 Vpp in several independent channels (up to 12), and with a maximum central frequencies of 1 MHz. In addition, it is able to work in several tests modes such as (1) pitch-catch, i.e., emitting in one channel and receiving in the rest of the channels, (2) pulse-echo, i.e., emitting and receiving in the same channels, or (3) beamforming, i.e., emitting from all the channels with a specific time-delay to obtain a directional effect in the transmission of guided waves. These kind of SHM systems have the potential to change the conservative and preventive maintenance into condition-based maintenance (CBM). This transformation may imply important economical and safety-related benefits by reducing redundancies with other NDE techniques in the inspection and by lively adapting the maintenance plan towards the actual health state of the structure. For instance, the cost of the inspections performed nowadays by the operator in stiffened aeronautical panels is 250 Euro/hour approximately, which could be dramatically reduced if a reliable and accurate SHM system drove the maintenance. One of the factors that influence the CBM is the earliness in the detection and diagnosis of the damage. To this end, nonlinear ultrasonic techniques have shown the potential to provide the aforementioned early indicators of damage, e.g. by detecting thermal fatigue degradation in composite materials [31]. More reliable and accurate models are expected to be obtained through the development of these types of nonlinear ultrasonic techniques. Therefore, the enhancement in damage diagnosis and prognostics by making use of nonlinear techniques and state-of-the-art SHM ultrasound systems, may lead to a desirable condition-based maintenance in the aerospace industry.

Wave based damage detection methods are based on calculating the reflection and transmission coefficients at the point of inhomogeneity. Evaluation of waves interaction coefficients in structural waveguides has been evaluated using various numerical methods, such as, spectral element methods [32], boundary element methods [33], decomposition [34], and probabilistic optimization [35] methods. The Finite Element (FE) based wave propagation analysis within periodic structures was first introduced in [36] to predict the wave dispersion characteristics within the layered media

over a wide frequency range. This was extended to 2D periodic structures in [36]. The computational efficiency of the method, as well as the post-processing scheme of its eigenproblem solutions were further improved through a new approach, the wave and finite element (WFE) method, introduced in [37]. The WFE has recently found application in predicting the vibroacoustic and dynamic properties of composite panels and shells [38, 39] with pressurised structure [40] having been investigated. The approach has also been employed in order to compute the reflection and transmission coefficients of waves impinging on joints of finite dimensions [41, 42].

Nonlinear wave interaction with crack-like defect has been studied numerically by FE using unilateral contact law with or without Coulomb friction for isotropic solid [43, 44]. These contact laws are available in commercial FE package and have also been used to study nonlinear wave interaction with delamination in composites waveguides [45] and with breathing [19] and buried [46] cracks in isotropic plate. However in [19], multi-mode guided wave is excited at the transmitter sensor. These modes may not have been fully separated when being received at the receiver sensor, especially when the sensor is close to the damage zone. Hence, this may lead to modes overlapping (mix-mode effect). Also in [46], it was presented that the wave frequency spectrum of the wave packet corresponding to the incident wave (in the nonlinear interaction with a crack) is nonlinear, i.e. contains harmonics. Physically, this is expected to be purely linear (such as in [43, 45]) because the incident wave has not come into contact with the nonlinear damage at that stage. Generation of harmonics is only valid for the new wave packet formed from the interaction phenomenon. Lastly, most of the reported work did not consider quantification of the harmonic reflection/transmission coefficients of the nonlinear wave-damage interaction phenomenon.

The main novelty of this work is the development of a generic WFE based computational scheme for computing wave interaction with localised nonlinear structural damage (LNSD) in arbitrarily layered composite structures. It is also aimed at establishing the computed harmonic wave interaction coefficients as a damage mode identification tool. More specifically, through-thickness mode-shapes of the guided waves propagating along structures of arbitrary layering and geometric complexities are obtained through a wave finite element method. In order to generate a specific guided mode, the WFE obtained through-thickness amplitudes relating to the eigen-properties of each mode are applied in a time domain FE calculation. The approach presents a significant ad-

vantage in specific mode excitation without mix-mode effect. The clapping mechanism of the LNSD is modelled using an element birth and death criterion. Two generic damage orientations, namely crack (vertical orientation) and delamination (horizontal orientation), are considered in this study. The guided wave propagates and interacts with the LNSD along the structure, and harmonic reflection coefficients are obtained from the interaction phenomenon. The calculated harmonic reflection coefficients are applied as indices for detecting presence of LNSD and to study the dependence of the interaction coefficients on the LNSD severity. Further analysis is also made into identification/classification of structural damage type based on their wave interaction coefficients magnitudes.

The remainder of this article is organized as follows: Section 2 presents the WFE based methodology for computing wave interaction with nonlinear damage. Section 3 presents numerical case studies together with discussion of the findings. Finally, Section 4 presents concluding remarks of the work.

2. Wave interaction with localised nonlinear structural damage

2.1. Wave constants calculation by a wave FE method

Elastic wave propagation in a composite structural waveguide, which is arbitrarily layered, and periodic in the x direction (Figure 1), is considered.

[Figure 1 about here.]

The propagation constants of the waves travelling through the waveguide is sought through a wave finite element method. Segment of the periodic waveguide is meshed along the axis of wave propagation as shown in Figure (1). The left and right hand sides of the segment both have the same number of nodes and degrees of freedom (DOFs) [47]. The problem can be condensed using the transfer matrix approach [48].

Assuming time-harmonic behaviour and neglecting structural damping, the governing equation of a FE modelled structural segment is

$$[\mathbf{K} - \omega^2\mathbf{M}]\mathbf{q} = \mathbf{f} \tag{1}$$

where $\mathbf{K}$ and $\mathbf{M}$ are the stiffness and mass matrices of the FE model for each considered frequency ω, and $\mathbf{q}$ and $\mathbf{f}$ the vectors of the nodal displacement and force of the segment.

The frequency dependent dynamic stiffness matrix (DSM) of the segment can be partitioned into its left, right and internal DoFs as

$$\begin{bmatrix} \mathbf{D}_{LL} & \mathbf{D}_{LI} & \mathbf{D}_{LR} \\ \mathbf{D}_{IL} & \mathbf{D}_{II} & \mathbf{D}_{IR} \\ \mathbf{D}_{RL} & \mathbf{D}_{RI} & \mathbf{D}_{RR} \end{bmatrix} \begin{Bmatrix} \mathbf{q}_L \\ \mathbf{q}_I \\ \mathbf{q}_R \end{Bmatrix} = \begin{Bmatrix} \mathbf{f}_L \\ \mathbf{f}_I \\ \mathbf{f}_R \end{Bmatrix} \tag{2}$$

Assume no external force is exerted on the internal nodes ($\mathbf{f}_I = 0$), classical condensation techniques [49], such as a dynamic condensation, is applied to condense the internal DoFs entries as

$$\begin{bmatrix} \mathbf{D}_{LL} - \mathbf{D}_{LI}\mathbf{D}_{II}^{-1}\mathbf{D}_{IL} & \mathbf{D}_{LR} - \mathbf{D}_{LI}\mathbf{D}_{II}^{-1}\mathbf{D}_{IR} \\ \mathbf{D}_{RL} - \mathbf{D}_{RI}\mathbf{D}_{II}^{-1}\mathbf{D}_{IL} & \mathbf{D}_{RR} - \mathbf{D}_{RI}\mathbf{D}_{II}^{-1}\mathbf{D}_{IR} \end{bmatrix} \begin{Bmatrix} \mathbf{q}_L \\ \mathbf{q}_R \end{Bmatrix} = \begin{Bmatrix} \mathbf{f}_L \\ \mathbf{f}_R \end{Bmatrix} \tag{3}$$

$$\begin{bmatrix} \mathbf{D}^*_{LL} & \mathbf{D}^*_{LR} \\ \mathbf{D}^*_{RL} & \mathbf{D}^*_{RR} \end{bmatrix} \begin{Bmatrix} \mathbf{q}_L \\ \mathbf{q}_R \end{Bmatrix} = \begin{Bmatrix} \mathbf{f}_L \\ \mathbf{f}_R \end{Bmatrix} \tag{4}$$

where the matrix $\mathbf{D}^*$ is the reduced dynamic stiffness matrix. Therefore, the continuity condition and equilibrium of forces equations, at the interface of two consecutive periodic segments r and $r+1$, are given as

$$\begin{aligned} \mathbf{q_R}^{(r)} &= \mathbf{q_L}^{(r+1)} \\ \mathbf{f_R}^{(r)} &= -\mathbf{f_L}^{(r+1)} \end{aligned} \tag{5}$$

Combining Eqs. (4) and (5), gives the relation of the displacement and force vectors of the left hand side and the right hand side of the segment as

$$\begin{Bmatrix} \mathbf{q_R}^{(r)} \\ \mathbf{f_R}^{(r)} \end{Bmatrix} = \begin{Bmatrix} \mathbf{q_L}^{(r+1)} \\ -\mathbf{f_L}^{(r+1)} \end{Bmatrix} = \mathbf{T} \begin{Bmatrix} \mathbf{q_L}^{(r)} \\ \mathbf{f_L}^{(r)} \end{Bmatrix} \tag{6}$$

where matrix $\mathbf{T}$ is the transfer matrix expressed as

$$\mathbf{T} = \begin{bmatrix} -\mathbf{D}_{LR}^{*\,-1}\mathbf{D}_{LL}^{*} & \mathbf{D}_{LR}^{*\,-1} \\ -\mathbf{D}_{RL}^{*} + \mathbf{D}_{RR}^{*}\mathbf{D}_{LR}^{*\,-1}\mathbf{D}_{LL}^{*} & -\mathbf{D}_{RR}^{*}\mathbf{D}_{LR}^{*\,-1} \end{bmatrix} \tag{7}$$

As the wave is propagating only in the x-direction, a constant of propagation, $\lambda = e^{-ikL_x}$ (where k is the wavenumber), relates the left side's displacement and internal force of the segment to that of the right side according to the Bloch's theorem [50] as

$$\begin{aligned} \lambda \mathbf{q}_L{}^{(r)} &= \mathbf{q}_R{}^{(r)} \\ -\lambda \mathbf{f}_L{}^{(r)} &= \mathbf{f}_R{}^{(r)} \end{aligned} \tag{8}$$

Combining Eqs. 6 and 8, the free wave propagation can be defined by the eigenvalue problem

$$\mathbf{T} \begin{Bmatrix} \mathbf{q}_\mathbf{L}{}^{(r)} \\ \mathbf{f}_\mathbf{L}{}^{(r)} \end{Bmatrix} = \lambda \begin{Bmatrix} \mathbf{q}_\mathbf{L}{}^{(r)} \\ \mathbf{f}_\mathbf{L}{}^{(r)} \end{Bmatrix} \tag{9}$$

whose eigenvalues λ_ω and eigenvectors $\boldsymbol{\phi}_\omega = \begin{Bmatrix} \boldsymbol{\phi}_q \\ \boldsymbol{\phi}_f \end{Bmatrix}_\omega$ solution sets provide a comprehensive description of the propagation constants and the wave mode shapes for each of the elastic waves propagating in the structural waveguide at a specified angular frequency ω. Both the positive going (with λ_ω^+ and $\boldsymbol{\phi}_\omega^+$) and negative going (with λ_ω^- and $\boldsymbol{\phi}_\omega^-$) waves are sought through the eigensolution. Positive going waves are characterised [48] by

$$\begin{aligned} |\lambda_\omega^+| &\leq 1 \\ \Re(\mathrm{i}\omega \boldsymbol{\phi}_f^{+\mathsf{T}} \boldsymbol{\phi}_q^+) &< 0 \text{ if } |\lambda_\omega^+| = 1 \end{aligned} \tag{10}$$

which states that when a wave is propagating in the positive x direction, its amplitude should be decreasing, or that if its amplitude is constant (in the case of propagating waves with no attenuation), then there is time average power transmission in the positive direction.

2.2. Localised nonlinear structural damage modelling

2.2.1. Harmonics generation through contact acoustic nonlinearity

In this work, wave interaction with nonlinear structural damage is examined. Contact acoustic nonlinearity (CAN) is generated when a propagating wave interacts with nonlinear/micro damage

within a structural medium. This leads to a clapping mechanism of the damage being activated during the interaction. Wave interaction with a clapping defect, which opens and closes alternatively, leads to the generation of sub and higher harmonic waves. Hence, sub and higher order terms are added to the convectional elastic Hooke's relation ($\sigma = E\varepsilon$) of the medium as

$$\sigma = E\varepsilon + \alpha E\varepsilon^2 + \beta E\varepsilon^3 + O(\varepsilon^4) + \alpha_0 E\varepsilon^{1/2} + \beta_0 E\varepsilon^{1/3} + O(\varepsilon^{1/4}) \tag{11}$$

Consider a nonlinear dynamic system of the form

$$\Upsilon(u) = \chi u + \alpha\chi u^2 + \beta\chi u^3 + \cdots + \alpha_0\chi u^{1/2} + \beta_0\chi u^{1/3} + \cdots \tag{12}$$

The input function of the system can be expressed in harmonic form as

$$u(\omega) = u_0 \mathrm{e}^{\mathrm{i}\omega t} \tag{13}$$

and then substitute the input function (Eq. 13) into the dynamic system (Eq. 12) to obtain the harmonic output of the system as

$$\Upsilon(u) = A_1 u(\omega) + A_2 u(2\omega) + A_3 u(3\omega) + O(4\omega) + B_1 u(\omega/2) + B_2 u(\omega/3) + O(\omega/4) \tag{14}$$

This shows that, apart from the fundamental harmonic, the output of a nonlinear dynamic system contains both sub ($\omega/2$, $\omega/3$, $\omega/4\cdots$) and super (2ω, 3ω, $4\omega\cdots$) order harmonics whereas the input contains only the fundamental harmonic (ω). Hence, wave interaction with nonlinear damage is expected to generate interaction coefficients not only at fundamental frequency but also at sub harmonic and super harmonic frequencies. This feature is highly essential in accessing localised nonlinearity within structural systems. As will be demonstrated in later sections, it is also essential for damage detection and identification.

2.2.2. Element birth/death criterion

As demonstrated above, harmonics are generated when waves propagating through a structural medium interact with nonlinear material behaviour such as contact-type defects like microscopic

breathing or clapping structural cracks, delaminations and unbonds. The nonlinear opening and closing of the defect as wave travels through it is based on the contact acoustic nonlinearity (CAN) phenomenon. The defect closes (full contact) during the compressional phase of the wave, and opens (full opening) during tensile phase as shown in Figure 2.

[Figure 2 about here.]

In CAN, compressive stress strengthens the contact between interface surfaces of the defect while tensile stress weakens it. Hence, the compressional phase of the wave penetrates the defect and closes it while the tensile part does otherwise.

Opening and closing of the clapping damage is a cyclic process. Through the elements birth/death criterion, elements within the damage zone are deactivated (damage opens) when their cumulative strains are positive (i.e. when undergoing tension) and reactivated (damage closes) when negative (i.e. when undergoing compression).

It is noted that when elements are deactivated, they are not removed or deleted from the structural model, but rather made insignificant in the model. Hence, during this stage, the material stiffness of the deactivated finite elements is reduced by a severe reduction factor [51]. This leads to an updated stiffness matrix in order to accommodate reduction in stiffness properties of the medium. As structural matrices (mass, stiffness or damping) are an assemblage of constituent elements matrices, the stiffness matrix of the affected elements is updated as

$$\boldsymbol{K}_u^e = \mu \boldsymbol{K} \tag{15}$$

where $\boldsymbol{K}$ is the original stiffness matrix of the elements when active (alive), $\boldsymbol{K}_u^e$ the updated stiffness matrix of the elements when deactivated (dead) and μ the reduction factor (equals 10^{-6} by default or a user defined value, typically $\ll 1$).

On the other hand, the mass matrix of the deactivated elements are set to zero to remove their effect from the entire model.

[Figure 3 about here.]

As earlier stated, deactivation of the elements within the damage zone depends on the cumulative strain value of the elements. The cumulative strain of the damage zone elements, as illustrated in Figure 3, are determined as

$$\varepsilon_d = \sum_{n=1}^{N} \varepsilon_{dn}$$
$$\varepsilon_b = q_2 - q_1 \tag{16}$$

with all strain values measured in the axis of excited wave-mode.

The iterative procedure of the elements birth/death criterion for nonlinear wave interaction modelling is summarised in the pseudocode presented in Algorithm 1.

Algorithm 1 Iterative procedure of the element birth/death criterion

1: Build the model, apply load and constraints and determine solution parameters
2: $i \leftarrow 1$ (first solution step)
3: Solve the model for solution step i
4: Determine ε_d and ε_b
5: **if** $\varepsilon_d < 0 \cap \varepsilon_b < 0$ **then**
6: Reactivate the damage zone elements if presently deactivated
7: **else**
8: Deactivate the damage zone elements if presently active
9: **end if**
10: **if** $i \leq m$ (where m equals number of solution steps) **then**
11: $i \leftarrow i + 1$ (next solution step)
12: Go to step 3
13: **else**
14: End of iteration
15: **end if**

The algorithm presents the routine through which the elements within the damage zone are systematically made active or inactive during the nonlinear transient analysis. After each solution step, the cumulative strains $(\varepsilon_d, \varepsilon_b)$ of the damage zone elements are calculated (Eq. 16). The

elements are made inactive if the magnitudes of the strains are positive (i.e. under tension) or active if the strain values are negative (i.e. under compression). This iteration is repeated for every load step of the analysis.

2.3. Finite element wave interaction modelling

Each WFE computed (presented in Section 2.1) propagating wavemode w with $w \in [1 \cdots W]$ in the structural waveguide can be grouped as

$$\begin{aligned} \boldsymbol{\Phi}_q^+ &= \begin{bmatrix} \boldsymbol{\phi}_{q,1}^+ & \boldsymbol{\phi}_{q,2}^+ & \cdots & \boldsymbol{\phi}_{q,W}^+ \end{bmatrix} \\ \boldsymbol{\Phi}_f^+ &= \begin{bmatrix} \boldsymbol{\phi}_{f,1}^+ & \boldsymbol{\phi}_{f,2}^+ & \cdots & \boldsymbol{\phi}_{f,W}^+ \end{bmatrix} \\ \boldsymbol{\Phi}_q^- &= \begin{bmatrix} \boldsymbol{\phi}_{q,1}^- & \boldsymbol{\phi}_{q,2}^- & \cdots & \boldsymbol{\phi}_{q,W}^- \end{bmatrix} \\ \boldsymbol{\Phi}_f^- &= \begin{bmatrix} \boldsymbol{\phi}_{f,1}^- & \boldsymbol{\phi}_{f,2}^- & \cdots & \boldsymbol{\phi}_{f,W}^- \end{bmatrix} \end{aligned} \tag{17}$$

The displacement eigenvectors of each positive going elastic wave $\boldsymbol{\phi}_{q,w}^+$ can be further grouped as

$$\boldsymbol{\phi}_{q,w}^+ = \begin{Bmatrix} \boldsymbol{q}_{1,x} & \boldsymbol{q}_{1,y} & \boldsymbol{q}_{2,x} & \boldsymbol{q}_{2,y} & \cdots & \boldsymbol{q}_{p,x} & \boldsymbol{q}_{p,y} \end{Bmatrix}^\mathsf{T} \tag{18}$$

with $\boldsymbol{q}_{p,x}$ and $\boldsymbol{q}_{p,y}$ the in-plane (x-axis) and the out-of-plane (y-axis) displacement components of node p where $p \in [1 \cdots P]$. P being the number of nodes along the lateral axis of the structural waveguide as shown in Figure 1. Hence, the displacement vectors of each propagating wave, in the in-plane $\boldsymbol{\phi}_{q,wx}^+$ and out-of-plane $\boldsymbol{\phi}_{q,wy}^+$ directions, can be extracted from Eqs. (17) and (18).

FE modelling of wave interaction with nonlinear damage in a layered composite plate is simulated using transient piezo-electrically generated ultrasonic wave. PZT wafer transducers are bonded to the plate as shown in Figure 8. The wafers and the plate are assumed to be of infinite dimension in the z direction (plane strain condition). In order to generate ultrasonic wave of a specific mode and avoid mix-mode effect, the transmitter PZTs are excited employing the WFE computed displacement of the mode. This will suppress other modes propagating through the waveguide.

Spatial (element size) and temporal (integration time step) resolutions of the FE model are chosen, to ensure solution convergence while ensuring the model computational size is relatively

reasonable, as

$$t_s = \frac{1}{20 f_{max}}; \qquad l_e = \frac{\lambda_{min}}{20} \tag{19}$$

Element size, l_e, is chosen to ensure that the FE discretization has at least 20 nodes per minimum wavelength. This discretisation is sufficiently adequate to avoid spatial aliasing and ensure the accuracy of higher harmonics [52]. The smaller the integration time step t_s, the better the accuracy of the numerical result. However, too small t_s requires high calculation time and hence increases computational cost excessively. Therefore the Newmark integration time scheme is employed to strike a compromise between the time step and the computational size using 20 points per cycle of the highest frequency of interest [52].

3. Case studies

3.1. Experimental validation

The computational scheme exhibited in this study is applied in a notched plate shown in Fig. 4. The plate, which is made of aluminium (E = 68.95 GPa, ρ = 2600 kg/m^3 and ν = 0.3), is 1.2 m long, 0.7 m wide and 0.002 m thick. The rectangular notch is machined at 0.7 m from the left edge of the plate and runs transversely through the width. A range of notches of different widths and depths are studied. The notch widths considered are within the range of 0.5 and 5.0 of the plate thickness at depths of 25% and 50% of the plate thickness.

[Figure 4 about here.]

In order to validate the presented scheme, the results derived through the scheme are compared against those obtained through experimental measurements and those of the WFE-FE methodology presented in [42].

[Figure 5 about here.]

The test rig set-up for the experimental measurements is shown in Fig. 5. At a given frequency, there exist at least two Lamb modes propagating through an aluminium plate [53]. However, single mode excitation and monitoring make wave interaction measurement easier and more accurate

without mixed-mode effect. Due to its simple and non-dispersive characteristics at low frequencies, the set-up is designed with the aim of exciting and receiving just symmetric lamb wave mode. This is achieved by sticking two piezoelectric transducers (referred to as the transmitter PZT) on the double surface at the excitation point, with the two actuators having same coordinates as shown in Fig. 4. Exciting these two transmitter PZTs with the same input signal, symmetric mode will be generated, while the antisymmetric mode will be suppressed. Similar approach can be applied to excite only antisymmetric mode, but with the directions of the input signals in opposite sense to each other. Two additional piezoelectric transducers (referred to as the receiver PZT) are bonded on the plate at 0.5 m and 0.9 m to respectively receive the reflected and transmitted wave signals from the notch.

The set-up system is composed of a dual channel Keysight 33512B arbitrary waveform generator, a Tabor 9200A high-voltage amplifier, with a gain factor of 40 dB, a DSOX2014A digital storage oscilloscope of sampling frequency 9.6 MHz and a PC. Circular radial mode piezoelectric transducers (Steminc part number: SMD07T02R412WL) are chosen to uniformly excite and register the guided waves. Each measurement corresponded to average of 32 tests in order to reduce the system noise. Using the waveform generator, a 10 V peak-to-peak 5-cycle Hanning window modulated tone-burst voltage signal is generated and applied to the two transmitter PZTs. The centre frequency of the excitation tone-burst being 200 KHz. Upon the excitation, elastic waves are generated by the transmitter transducers and sent through the plate. The voltage output of the travelling waves are measured at the receiver PZT using the oscilloscope. The PZT to the left side of the damage measures the reflected signal from the damage, while that to the right side of the damage measures the transmitted signal. The received signal is amplified and input to the oscilloscope for digital capture and display on the PC.

[Figure 6 about here.]

The waveform of the reflected output signal after interaction with the notch in the damaged plate is presented in Fig. 6. The notch in this case is 1 mm deep and 5 mm wide. The output signal waveform is superimposed with that measured from the damage free (pristine) plate. It can be observed from Fig. 6 that, compared with the pristine plate waveform history, there exist a new

wave packet generated in the damage plate waveform history. It therefore follows that the new signal packet is generated by an interaction of the travelling wave with the notch. Another evident difference is that the damaged plate signal has a slight phase shift and amplitude drop which can be attributed to energy leakage during generation of the new signal packet.

FFT of the measured responses is conducted to obtain the frequency spectral of the output signals. Unwanted signals such as the edge reflections are gated out during the FFT analysis. The wave reflection coefficient is therefore calculated by dividing the frequency spectrum of the reflected signal by that of the incident signal.

[Figure 7 about here.]

The superimposed results of the presented approach, experimental measurements and WFE-FE methodology [42] are shown in Fig. 7. The results present wave reflection coefficients, at fundamental frequency, as a function of the notch width for notch depths of 25% and 50% of the plate thickness. The notch width axis is normalised to the plate thickness, so that the results may be applied equally to other thicknesses of the plate provided that the frequency-thickness of 400 KHz-mm is also maintained. The reflection coefficient magnitude in each case increases with respect to the notch width until a width of about 3.0 of the plate thickness. Beyond this level, the coefficient magnitude decreases with respect to notch width until it tends towards zero value, and then increases again in a sinusoidal-like fashion.

As shown in Fig. 7, results obtained by the presented scheme agree very well with the experimental measurements with a maximum difference of about 6%. Compared with the WFE-FE predictions, the difference rises to about 18%. This difference can be attributed to energy leakage to higher harmonics in the nonlinear analysis. It should be noted that the WFE-FE model is a linear wave interaction analysis with no leakage of energy to harmonics generation. Hence, the higher difference.

3.2. Numerical case studies

The capability of the presented scheme for computing nonlinear wave interaction phenomenon is exhibited in this section. Two different LNSDs, namely crack and delamination, are considered.

In each case, pristine plate, plate with LLSD and plate with LNSD are all considered in order to distinguish wave interaction phenomenon in each scenario of structural condition. Response of each failure mode to the interaction phenomenon is also being studied and analysed.

3.2.1. Description and boundary condition of the model

A sandwich composite plate of thickness 2 mm and length $l_p = 1000$ mm is considered as shown in Fig. 8. The viscoelastic sandwich plate is made of a glass/fibre core (of material properties $E_x = 45$ GPa, $E_y = 16$ GPa, $E_z = 16$ GPa, $G_{xy} = 5.83$ GPa, $G_{yz} = 5.79$ GPa, $G_{xz} = 5.83$ GPa, $\nu_{xy} = 0.28$, $\nu_{yz} = 0.4$, $\nu_{xz} = 0.28$, $\rho = 1400$ kg/m^3) sandwiched between isotropic skins (of properties $E = 208$ GPa, $\nu = 0.3$, $\rho = 7800$ kg/m^3). The thickness of the core $h_c = 1.6$ mm while that of each skin $h_s = 0.2$ mm. Three piezoelectric sensors, namely transmitter and receiver PZTs, each of length 7 mm and thickness 0.2 mm are bonded on the plate as shown in Fig. 8. Material properties of the piezoelectric are: elastic flexibility: ($S_{11} = S_{33} = 16.4$, $S_{22} = 18.8$, $S_{12} = S_{21} = -7.22$, $S_{13} = S_{31} = -5.74$, $S_{23} = S_{32} = -7.22$, $S_{44} = S_{55} = 47.5$, $S_{66} = 44.3$) $\times$ 10^{-12} m^2/N, piezoelectric strain coefficients: ($d_{21} = -1.71$, $d_{22} = 3.74$, $d_{23} = -1.71$, $d_{14} = 5.84$, $d_{35} = 5.84$) $\times$ 10^{-10} m/V, electric permittivity: ($\varepsilon_{11} = \varepsilon_{33} = 2.12$, $\varepsilon_{22} = 1.75$) $\times$ 10^{-8} F/m. The piezoelectric has a loss tangent of 0.02 and a density of 7750 kg/m^3.

[Figure 8 about here.]

FE calculations are performed in two-dimensional domain using rectangular plane strain elements. The elements have two DoFs in each node; displacements in x and y directions. ANSYS 14.0 is used for the FE modelling. 2-D 4-node PLANE182 (for the plate) and PLANE13 (for the PZTs) elements are chosen due to their plane strain capability in modelling structural solids.

Eq. (9) is solved for the wave propagation constants. Two propagating waves, longitudinal (symmetric mode) and bending (antisymmetric mode), are obtained. The WFE calculated displacement mode shapes of the propagating waves in the in-plane and out-of-plane directions are presented in Fig. 9.

[Figure 9 about here.]

In general, as presented in Section 2.3, the WFE computed wave modes obtained across the thickness of the plate at one of its extreme cross-sections can be excited one-by-one in the FE calculation as time-dependent harmonic voltage boundary conditions (of excitation frequency ω). In this study, the longitudinal guided wave is generated and applied on the transmitter PZTs (as shown in Fig. 8) to produce a longitudinal wave motion. The excitation signal is a 20 V peak-to-peak hanning windowed toneburst consisting of five cycles at center frequency of $\omega = 100$ kHz and longitudinal wave amplitude $\boldsymbol{\phi}^{+}_{q,wx}$. The time dependent harmonic voltage is given as

$$V(t) = \begin{cases} \phi^{+}_{q,wx} \sin(\omega t) \cdot (0.5 - 0.5\cos(\frac{\omega t}{5}), & t \leq \frac{10\pi}{\omega} \\ 0, & t > \frac{10\pi}{\omega} \end{cases} \tag{20}$$

Exciting both transmitter PZTs (as shown in Fig. 8) with the WFE calculated mode shape of the considered guided mode will only excite the particular guided mode, with the other mode being suppressed. This approach aids independent excitation of a guided mode thereby avoiding mix-mode effect in the analysis.

3.2.2. Pristine plate

The plate in its undamaged state is first considered as a baseline for other conditions to be considered.

Fig. 10 presents the calculated time history of the signal, obtained at the receiver PZT, for the undamaged plate. As observed, there exist a single wavelet in the predicted response which suggests that the wave interact with no form of damage/discontinuities during propagation along the plate. Frequency spectrum (Figs. 12 and 16) of the wavelet also gives only the fundamental frequency component which ascertain the absence of any form of nonlinearity in the pristine plate.

3.2.3. Interaction with crack

In order to exhibit the effect of crack severity on the wave interaction phenomenon, interaction coefficients are obtained as a function of the crack depths. Crack depths considered include 0.2, 0.4, 0.6, 0.8, 1.0, 1.2, 1.4 and 1.6 (all in millimetre). These correspond to 0.1 to 0.8 of the plate thickness. The crack severity is scaled to normalise the crack depth to the plate thickness, so

that the results obtained can be applied equally to other thicknesses of the plate provided that the frequency-thickness of 200 kHz-mm is satisfied.

In each case, the crack is situated at 600 mm from the transmitter PZT, and reflection from the crack-damage interaction is received at the receiver PZT located 100 mm away from the crack. The configuration is as shown in Fig. 8a.

As earlier informed, calculations are made for plate with linear crack and plate with nonlinear crack in order to distinguish wave interaction phenomenon in each scenario of structural condition.

3.2.3.1 Interaction with localised linear crack

Guided wave interaction with localised linear crack within the sandwich plate is considered in this section. In this case, the crack opens throughout the calculation window.

[Figure 10 about here.]

[Figure 11 about here.]

The time domain response of the plate with linear crack is presented in Fig. 10. Compared to the pristine plate, there exist two wavelets; the incident wavelet and the wavelet reflected from the wave-crack interaction phenomenon. The presence of the reflected wavelet is an indication of damage, in the structural waveguide, which interact with the wave during propagation. This confirms the capability of the developed scheme in detecting structural damage.

[Figure 12 about here.]

Fig. 12 presents the frequency spectral for the incident wavelet (Fig. 12a), when the reflected wavelet ($t \geq 145\ \mu s$) is gated out, and for the reflected wavelet (Fig. 12b), when the incident wavelet ($t \leq 145\ \mu s$) is gated out. However, as in the pristine plate, there exist spectrum component for only the fundamental frequency for both the incident and the reflected wavelets. The absence of harmonics signifies an absence of nonlinearity in the waveguide with linear crack.

[Figure 13 about here.]

Wave interaction reflection coefficient is estimated by dividing the reflected response signal by the incident response signal. Fig. 13 presents the reflection coefficients for the damage interaction in the linear domain. In order to further validate the presented methodology, the results presented are compared against the approach presented in [42] for a sandwich plate with linear structural crack. Excellent agreement is observed for the wave interaction coefficients obtained by both methodologies.

3.2.3.2 Interaction with localised nonlinear crack

Guided wave interaction with localised nonlinear crack within the sandwich plate is considered in this section. In this case, the crack opens and closes under tension and compression respectively.

The time history of the response obtained for the plate with nonlinear crack at crack depth 0.3 of the plate thickness is presented in Fig. 11. Similar to the linear crack case, the response signal contains two wavelets; incident and reflected packets. But unlike the linear case, the reflected wave packet shows distortion along its path. This is due to contact acoustic nonlinearity within the waveguide.

Fig. 12 shows the frequency spectral for the incident wavelet (Fig. 12a) and the reflected wavelet (Fig. 12b) when the reflected and incident wavelets are respectively gated out. Compared to the linear case, the nonlinear wave interaction gives not only the fundamental frequency spectrum components but also sub and higher harmonic components up to the fifth harmonic. The presence of harmonic components is a significant indication of the presence of nonlinearity in the system. It should be noted that the amplitude of the spectrum at fundamental frequency is lower in the nonlinear case compared to the linear case. This is as a result energy leaking to higher harmonics in the nonlinear case. It should also be noted that the spectrum of the incident wave is purely linear (even for the nonlinear case), i.e. no generation of harmonics. This is because the wave has not interacted with the nonlinear crack at that stage.

[Figure 14 about here.]

The results of the fundamental and higher harmonic wave reflection coefficients as a function of the crack severity are presented in Fig. 14.

As expected, due to energy dissipation of the wave to generate higher harmonics, it is observed that the reflection coefficients reduces as the harmonic frequency increases. Peak reflection coefficient of about 0.76 is obtained at the fundamental harmonic, compared to 0.11, 0.066 and 0.027 obtained at the second, third and fourth harmonics respectively.

Except at fundamental frequency where the trend is almost linear with respect to the crack severity, the dependence of the reflection coefficient on the crack severity follows a quarter-sinusoidal profile. In each case, the reflection coefficient increases with the crack severity until about a crack severity of 0.7 of the plate thickness where the reflection coefficient starts reducing against the crack severity. The outcome of the wave reflection coefficient relationship with crack severity could, in principle, be used as an indicator for early monitoring and detection of a crack. This outcome could also be used to measure the span of a crack.

3.2.4. Interaction with delamination

In this case, interaction of guided wave with localised skin-core delamination is considered. Calculations are made for plate with linear crack and plate with nonlinear crack in order to distinguish wave interaction phenomenon in each scenario of structural condition.

In order to exhibit the effect of the delamination severity on the wave interaction phenomenon, interaction coefficients are obtained as a function of the delamination widths. Delamination widths of 0.2, 0.4, 0.6, 0.8, 1.0, 1.2, 1.4 and 1.6 (all in millimetre) are considered. These correspond to 0.1 to 0.8 of the plate thickness. The delamination severity is scaled to normalise the delamination width to the plate thickness, so that the results obtained can be applied equally to other thicknesses of the plate provided that the frequency-thickness of 200 kHz-mm is satisfied.

In each case, the delamination is situated at 600 mm from the transmitter PZT, and reflection from the guided wave interaction with the delamination is received at the receiver PZT located 100 mm away from the delamination. The configuration is as shown in Fig. (8b).

It should be noted that similar parameters and configurations used in the crack case are used in this case. This is done in order to directly compare and contrast results in both cases and exhibit the developed methodology as a damage identification tool.

3.2.4.1 Interaction with localised linear delamination

Guided wave interaction with localised linear delamination within the sandwich plate is considered in this section. As a linear analysis, the plate remains delaminated throughout the calculation window.

[Figure 15 about here.]

Fig. (15) presents the time domain response of the guided wave interaction with linear delamination within the plate superimposed with the time history obtained for the pristine plate.

The pristine plate response contains only the incident wavelet while the plate with linear delamination contains incident and reflected wavelets. The presence of the reflected wavelet is an indication of damage, in the structural waveguide, which interact with the guided wave during propagation. This establish the application of the developed scheme for damage detection.

[Figure 16 about here.]

The frequency spectrum of the incident wavelet, in the time history (Fig. 15) of the plate with linear delamination, when the reflected wavelet ($t \geq 145\ \mu s$) is gated out is shown Fig. (16a). As expected, the incident wave spectrum of the pristine plate and that of the plate with linear delamination are equal. The frequency spectrum of the reflected wavelet when the incident wavelet ($t \leq 145\ \mu s$) is gated out is shown in Fig. (16b). As observed, there exist spectrum component for only the fundamental harmonic. The absence of higher harmonics confirms the absence of nonlinearity in the plate with linear delamination.

3.2.4.2 Interaction with localised nonlinear delamination

Guided wave interaction with localised nonlinear delamination within the sandwich plate is considered in this section. Based on the developed scheme, the clapping delamination opens and closes under tension and compression respectively.

[Figure 17 about here.]

The time history of the response obtained for the plate with nonlinear delamination at delamination width 0.3 of the plate thickness is presented in Fig. 17. It is superimposed with the time history of the response obtained for the pristine plate.

Similar to the response obtained for the plate with linear delamination, the response contains two wave packets; incident and reflected packets. But unlike the linear case, the reflected wave packet of the nonlinear case shows distortion along its path. This is due to contact acoustic nonlinearity within the nonlinear system. The presence of the distorted reflected wave package is an indication of not just a damage but a nonlinear damage in the structural waveguide.

The frequency spectrum of the incident wave package and that of the reflected wave package, when the reflected ($t \geq 145\ \mu s$) and incident ($t \leq 145\ \mu s$) wave packages are respectively gated out, are presented in Fig. (16) for the sandwich plate with nonlinear delamination. The results presented are superimposed with that of the pristine plate and the plate with linear delamination. As observed from the presented results, the frequency spectrum of the incident wave equals to those obtained for the pristine plate as well as the plate with linear delamination. It should be noted that the spectrum is purely linear, i.e. no generation of harmonics is observed. This is because the wave has not interacted with the nonlinear delamination at that stage. However, the frequency spectrum of the reflected wave generates harmonic components up to the fifth harmonics. The presence of harmonic components in the frequency spectrum is a significant indication of the presence of nonlinearity in the system. It should also be noted that the amplitude of the spectrum component at fundamental frequency is lower in the nonlinear case compared to the linear case. This is as a result energy leaking to higher harmonics in the nonlinear case.

[Figure 18 about here.]

The results of the harmonic wave reflection coefficients, generated for the guided wave interaction with nonlinear delamination in the sandwich plate, as a function of the delamination severity are presented in Fig. 18.

As expected, due to energy dissipation of the wave to generate higher harmonics, it is observed that the reflection coefficients reduces as the harmonic frequency increases. Peak reflection coefficient of about 0.19 is obtained at the fundamental harmonic, compared to 0.056, 0.019 and

0.012 obtained at the second, third and fourth harmonics respectively. In relation to the delamination width severity, the reflection coefficient follows a quarter-sinusoidal profile. In each case, the reflection coefficient increases with the delamination severity until delamination of an average width of 0.7 of the plate thickness where the reflection coefficient starts reducing against the delamination severity. The outcome of the wave reflection coefficient relationship with delamination severity could, in principle, be used as an indicator for early monitoring and detection of a delamination. This outcome could also be used to measure the span of a delamination.

Having demonstrated the application of the developed scheme in detecting LNSD of different modes, it is essential to exhibit the applicability of the scheme in classifying/identifying the damage modes using the calculated harmonic reflection coefficients. Two modes (of different orientations) of the most common localised damage modes in periodic structures are considered; crack and delamination.

As presented and discussed above, the harmonic reflection coefficients of both damage modes follow similar relationship with respect to the span of the localised damage. However, as observed from the results, the reflection coefficient magnitudes are obviously different at various harmonic frequencies generated. Peak reflection coefficient magnitude of about 0.76 is obtained for the guided wave interaction with crack at fundamental harmonic compared to 0.19 obtained for interaction with delamination. Similarly, 0.11, 0.066 and 0.027 are obtained at second, third and fourth harmonics respectively for interaction with crack compared to 0.056, 0.019 and 0.012 respectively obtained for interaction with delamination. These depict an average difference of about 62% between the results obtained for the wave interaction with crack and that of delamination. Based on these outcomes, it is evident that the developed methodology can be applied to detect and quantify localised nonlinear structural damage (LNSD) in composite structures and classify them into specific mode.

4. Concluding remarks

A WFE-based computational scheme for analysing and quantifying wave interaction with nonlinear defects in composite structure is presented in this article. The scheme can be applied to structures of arbitrary complexity, layering and material characteristics as an FE discretisation

is employed. The scheme applies the WFE computed wave modes as time-dependent harmonic boundary conditions, using transient piezo-electrically generated ultrasonic wave, on the plate and is able to compute the generation of wave harmonics for each excited wave. In line with the identified research gaps highlighted in Sec. 1 and the main objectives of this work, the principal contributions of the work can be summarised as

(i) The presented scheme successfully models nonlinear damage using an element birth and death criterion in a commercial FE software.

(ii) The scheme is able to impose specific guided wave mode without a mix-mode effect due to the WFE-obtained mode displacement being employed.

(iii) The scheme successfully models wave propagation and interaction with nonlinear damage within a structural medium. As demonstrated through the obtained incident and reflected wave packets, the property of the wave remains linear until interaction with the nonlinearity within the medium. Upon interaction with the nonlinear damage, wave property becomes nonlinear with generation of harmonic reflected wave packets.

(iv) The scheme is also able to compute sub and super harmonic reflection coefficients for the guided wave interaction with nonlinear structural damage. Results obtained through the developed methodology are validated with experimental measurements and results presented in open literature for guided wave interaction with localised damage. Good agreement is obtained among the results.

(v) The dependence of the wave interaction coefficients on the severity of the nonlinear damage is analysed using crack and delamination as case studies.

(vi) The application of the developed scheme in classifying and identifying the detected damage mode using the quantified harmonic reflection coefficients is also demonstrated.

Future developments are focussing on modelling and implementing efficient multiscale damage models in order to accurately capture the nonlinear mechanics of advanced damage scenarios, while retaining the size of the FE model and computational effort at acceptable level.

5. Data availability

The raw/processed data required to reproduce these findings cannot be shared at this time as the data also forms part of an ongoing study. They will be made available upon request.

References

[1] M. Breazeale, D. Thompson, Finite-amplitude ultrasonic waves in aluminum, Applied Physics Letters 3 (1963) 77–78.

[2] A. Vakakis, Scattering of structural waves by nonlinear elastic joints, Journal of Vibration and Acoustics 115 (1993) 403–410.

[3] A. Nayfeh, A. Vakakis, T. Nayfeh, A method for analysing the interaction of nondispersive structural waves and nonlinear joints, The Journal of the Acoustical Society of America 93 (1993) 849–856.

[4] P. Nagy, Fatigue damage assessment by nonlinear ultrasonic materials characterisation, Ultrasonics 36 (1998) 375–381.

[5] D. Donskoy, A. Sutin, Vibroacoustic modulation nondestructive evaluation technique, Journal of Intelligent Material Systems and Structures 9 (1998) 765–771.

[6] M. Deng, Analysis of second-harmonic generation of lamb modes using a modal analysis approach, Journal of Applied Physics 94 (2003) 4152–4159.

[7] V. Zaitsev, V. Nazarov, V. Gusev, B. Castagnede, Novel nonlinear modulation acoustic technique for crack detection, NDT&E International 39 (2006) 184–194.

[8] V. Rao, E. Kannan, R. Prakash, K. Balasubramaniam, Fatigue damage characterisation using surface acoustic wave nonlinearity in aluminum alloy aa7175-t7351, Journal of Applied Physics 104 (2008) 123508–.

[9] H. Hu, W. Staszewski, N. Hu, R. Jenal, G. Qin, Crack detection using nonlinear acoustics and piezoceramic transducers instantaneous amplitude and frequency analysis, Smart Materials and Structures 19 (2010) 065017–.

[10] Z. Su, C. Zhou, M. Hong, L. Cheng, Q. Wang, X. Qing, Acousto-ultrasonic based fatigue damage characterisation: Linear versus nonlinear signal features, Mechanical Systems and Signal Processing 45 (2014) 225–239.

[11] H. Lim, H. Sohn, M. DeSimio, K. Brown, Reference free fatigue crack detection using nonlinear ultrasonic modulation under various temperature and loading conditions, Mechanical Systems and Signal Processing 45 (2014) 468–478.

[12] M. Scalenrandi, V. Agostini, P. Delsanto, K. Van Den Abeele, P. Johnson, Local interaction simulation approach to modelling nonclassical, nonlinear elastic behavior in solids, The Journal of the Acoustical Society of America 113 (2003) 3049–3059.

[13] P. Delsanto, A. Gliozzi, M. Hirsekorn, M. Nobili, A 2d spring model for the simulation of ultrasonic wave propagation in nonlinear hysteretic media, Ultrasonics 44 (2006) 279–286.

[14] C. Pecorari, Nonlinear interaction of plane ultrasonic waves with an interface between rough surfaces in contact, The Journal of the Acoustical Society of America 113 (2003) 3065–3072.

[15] A. Croxford, P. Wilcox, B. Drinkwater, P. Nagy, The use of non-collinear mixing for nonlinear ultrasonic dtection of plasticity and fatigue, The Journal of the Acoustical Society of America 126 (2009) 117–122.

[16] K. Kawashima, R. Omote, T. Ito, H. Fujita, T. Shima, Nonlinear acoustic response through minute surface cracks: Fem simulation and experimentation, The Journal of the Acoustical Society of America 40 (2002) 611–615.

[17] H. Soshu, S. Toshihiko, Detection of a closed crack by nonlinear acoustics using ultrasonic transducers. in review of progress in quantitative nondestructive evaluation, The Journal of the Acoustical Society of America 32nd ed. (2006) 277–282.

[18] V. Giurgiutiu, M. Gresil, B. Lin, A. Cuc, Y. Shen, C. Roman, Predictive modelling of piezoelectric wafer active sensors interaction with high frequency structural waves and vibration, Acta Mechanica 223 (2012) 1681–1691.

[19] Y. Shen, V. Giurgiutiu, Predictive modelling of nonlinear wave propagation for structural health monitoring with piezoelectric wafer active sensors, Journal of Intelligent Material Systems and Structures 25 (2014) 506–520.

[20] T. Autrusson, K. Sabra, M. Leamy, Reflection of compressional and rayleigh waves on the edges of an elastic plate with quadratic nonlinearity, The Journal of the Acoustical Society of America 131 (2012) 1928–1937.

[21] G. Fierro, F. Ciampa, D. Ginzgurg, E. Onder, M. Meo, Nonlinear ultrasonic modelling and validation of fatigue damage, Journal of Sound and Vibration 343 (2015) 121–130.

[22] N. Rauter, R. Lammering, T. Kuhnrich, On the detection of fatigue damage in composites by use of second harmonic guided waves, Composite Structures 152 (2016) 247–258.

[23] Y. Shen, V. Giurgiutiu, Predictive simulation of nonlinear ultrasonics, in: Proceedings of the Health Monitoring of Structural and Biological Systems Conference, pp. –.

[24] K. Jhang, Nonlinear ultrasonic techniques for nondestructive assessment of micro damage in material: a review, International Journal of Precision Engineering and Manufacturing 10 (2009) 123–135.

[25] I. Solodov, D. Doring, G. Busse, New opportunities for ndt using nonlinear interaction of elastic waves with defects, Journal of Mechanical Engineering 57 (2011) 169–182.

[26] D. Broda, W. Staszewski, A. Martowicz, T. Uhl, V. Silberschmidt, Modelling of nonlinear crack-wave interactions for damage detection based on ultrasound: a review, Journal of Sound and Vibration 333 (2014) 1097–1118.

[27] K. Matlack, J. Kim, L. Jacobs, J. Qu, Review of second harmonic generation measurement techniques for material state determination in metals, Journal of Nondestructive Evaluation 34 (2015) 1–23.

[28] G. Aranguren, P. Monje, V. Cokonaj, E. Barrera, M. Ruiz, Ultrasonic wave-based structural health monitoring embedded instrument, Review of Scientific Instruments 84 (2013) 125106–1 – 125106–7.

[29] A. Alcaide, E. Barrera, M. Ruiz, G. Aranguren, Damage detection on aerospace structures using pamela shm

system, in: 6th International Symposium on NDT in Aerospace, Madrid.

[30] P. M. Monje, L. Casado, G. Aranguren, V. Cokonaj, E. Barrera, M. Ruiz, Integrated electronic system for ultrasonic structural health monitoring, in: European workshop on structural health monitoring, pp. 1–8.

[31] W. Li, Y. Cho, J. D. Achenbach, Detection of thermal fatigue in composites by second harmonic lamb waves, Smart Materials and Structures 21 (2012).

[32] S. P. Shone, B. R. Mace, T. P. Waters, Reflection and transmission coefficients using the spectral element method: Application to crack modelling in beams., in: Proceedings of Institute of acoustics Spring Conference, Institute of Sound and Vibration Research, Southampton, UK, pp. –.

[33] X. G. Zhao, J. L. Rose, Boundary element modelling for defect characterization potential in a wave guide, International Journal of Solids and Structures 40 (2003) 2645–2658.

[34] M. Castaings, C. Le, B. Hosten, Modal decomposition method for modeling the interaction of lamb waves with cracks, The Journal of the Acoustical Society of America 112 (2002) 2567–2582.

[35] C. T. Ng, M. Veidt, H. F. Lam, Guided wave damage characterisation in beams utilising probabilistic optimisation, Engineering Structures 31 (2009) 2842–2850.

[36] D. Mead, A general theory of harmonic wave propagation in linear periodic systems with multiple coupling, Journal of Sounds and Vibration 27 (1973) 235–260.

[37] B. R. Mace, D. Duhamel, M. J. Brennan, L. Hinke, Finite element prediction of wave motion in structural waveguides, The Journal of the Acoustical Society of America 117 (2005) 2835–2843.

[38] R. Apalowo, D. Chronopoulos, M. Ichchou, Y. Essa, F. Martin De La Escalera, The impact of temperature on wave interaction with damage in composite structures, Proceedings of the Institution of Mechanical Engineers, Part C: Journal of Mechanical Engineering Science 231 (2017) 3042–3056.

[39] D. Chronopoulos, C. Droz, R. Apalowo, M. Ichchou, W. Yan, Accurate structural identification for layered composite structures, through a wave and finite element scheme, Composite Structures 182 (2017) 566–578.

[40] R. Apalowo, D. Chronopoulos, G. Tanner, Wave interaction with defects in pressurised composite structures, Journal of Nondestructive Evaluation 37 (2018) 48.

[41] J. M. Mencik, M. N. Ichchou, Multi-mode propagation and diffusion in structures through finite elements, European Journal of Mechanics-A/Solids 24 (2005) 877–898.

[42] J. M. Renno, B. R. Mace, Calculation of reflection and transmission coefficients of joints using a hybrid element/wave and finite element approach, Journal of Sound and Vibration 332 (2013) 2149–2164.

[43] P. Blanloeuil, A. Meziane, C. Bacon, Nonlinear interaction of ultrasonic waves with a crack of different orientations, in: AIP Conference Proceedings, pp. 99–106.

[44] P. Blanloeuil, A. Meziane, A. Norris, C. Bacon, Analytical extension of finite element solution for computing the nonlinear far field of ultrasonic waves scattered by a closed crack, Wave Motion 66 (2016) 132–146.

[45] R. Soleimanpour, C.-T. Ng, Locating delaminations in laminated composite beams using nonlinear guided

waves, Engineering Structures 131 (2017) 207–219.

[46] X. Wan, Q. Zhang, G. Xu, P. W. Tse, Numerical simulation of nonlinear lamb waves used in a thin plate for detecting buried micro-cracks, Sensors 14 (2014) 8528–8546.

[47] E. Manconi, B. R. Mace, Modelling wave propagation in two-dimensional structures using a wave/finite element technique, ISVR Technical Memorandum (2007).

[48] B. R. Mace, D. Duhamel, M. J. Brennan, L. Hinke, Finite element prediction of wave motion in structural waveguides, The Journal of the Acoustical Society of America 117 (2005) 2835–2843.

[49] W. X. Zhong, F. W. Williams, A. Y. T. Leung, Sympletic analysis for periodical electro-magnetic waveguides, Journal of Sound and Vibration 267 (2003) 227–244.

[50] F. Bloch, Über die quantenmechanik der elektronen in kristallgittern, Zeitschrift für physik 52 (1929) 555–600.

[51] I. ANSYS, ANSYS 14.0 User's Help, 2014.

[52] F. Moser, L. Jacobs, J. Qu, Modelling elastic wave propagation in waveguides with the finite element method, NDT&E International 32 (1999) 225–234.

[53] J. Nienwenhui, J. Neumann, D. Greve, I. Oppenheim, Generation and detection of guided waves using pzt wafer transducers, IEEE transactions on ultrasonics, ferroelectrics, and frequency control 52 (2005) 2103–2111.

List of Figures

1 FE mesh of section of the composite waveguide with the left and right sides nodes DoFs $\mathbf{q_L}$, $\mathbf{q_R}$ bullet marked and range of internal nodes DoFs $\mathbf{q_I}$ also illustrated (Not to scale) . . . 32
2 Acoustic mechanism in a contact-type defect: the defect opens under tension and closes when in compression phase . . . 33
3 Configuration of the element birth/death criterion for damage clapping mechanism: (a) Crack (b) Delamination. (Not to scale) . . . 34
4 Schematic representation of the notched plate set-up: (a) front view; (b) plan view 35
5 Assembly of the experimental configuration . . . 36
6 Superimposed experimental time record for pristine (-) and notched (. . .) plates. Notch is 1 mm deep and 5 mm wide . . . 37
7 Wave reflection coefficients from the notch as a function of the notch width/plate thickness: Current scheme (o), Experimental measurements (-), WFE-FE methodology [42] (*) . . . 38
8 Schematic of the FE calculation configuration for sandwich plates with (a) crack and (b) delamination . . . 39
9 Mode shapes of the propagating waves in the sandwich plate at 100 kHz; left column: in-plane, right column: out-of-plane. . . . 40
10 Superimposed time history predictions for the pristine plate ($\cdots$) and the plate with linear crack (-) . . . 41
11 Superimposed time history predictions for the pristine plate ($\cdots$) and the plate with nonlinear crack (-) . . . 42
12 Superimposed frequency spectral of the incident and the reflected wavelets: pristine plate (- -); plate with linear crack ($\cdots$); plate with nonlinear crack (-) . . . 43
13 Wave interaction reflection coefficients for the plate with linear crack: present methodology (-o); computation as in [42] ($*$) . . . 44
14 Wave interaction reflection coefficients for the plate with nonlinear crack at different harmonic frequencies . . . 45
15 Superimposed time history predictions for the pristine plate ($\cdots$) and the plate with linear delamination (-) . . . 46
16 Superimposed frequency spectral of the incident and the reflected wavelets: pristine plate (- -); plate with linear delamination ($\cdots$); plate with nonlinear delamination (-) . . . 47
17 Superimposed time history predictions for the pristine plate ($\cdots$) and the plate with nonlinear delamination (-) . . . 48
18 Wave interaction reflection coefficients for the sandwich plate with nonlinear delamination at different harmonic frequencies . . . 49

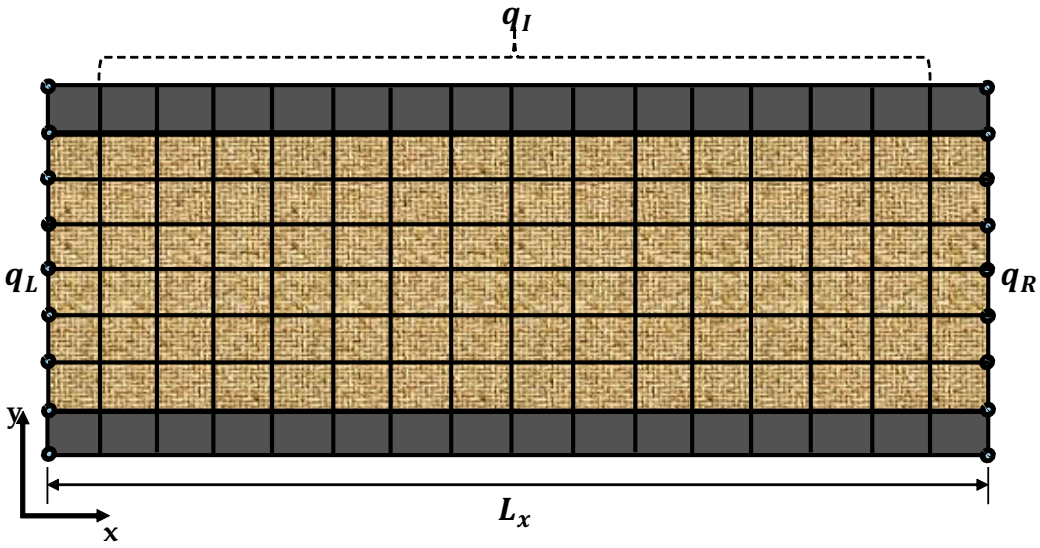

Figure 1: FE mesh of section of the composite waveguide with the left and right sides nodes DoFs $\mathbf{q_L}$, $\mathbf{q_R}$ bullet marked and range of internal nodes DoFs $\mathbf{q_I}$ also illustrated (Not to scale)

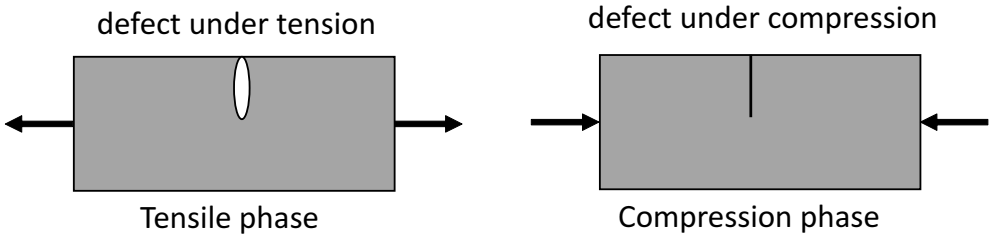

Figure 2: Acoustic mechanism in a contact-type defect: the defect opens under tension and closes when in compression phase

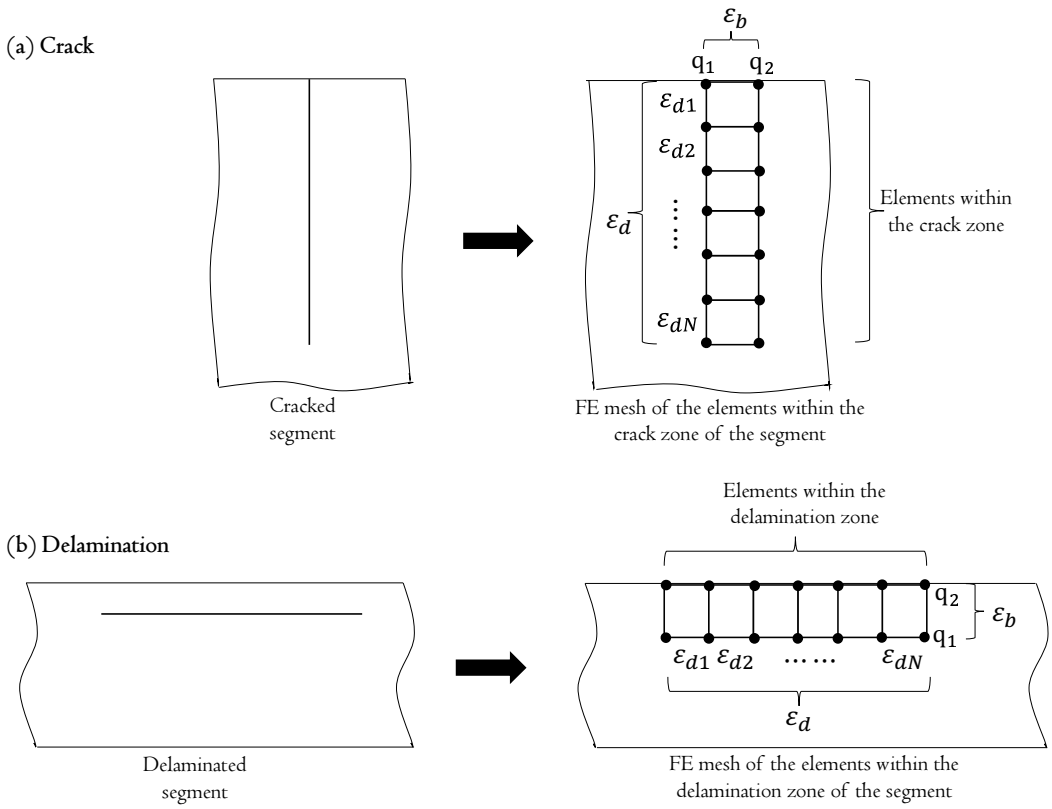

Figure 3: Configuration of the element birth/death criterion for damage clapping mechanism: (a) Crack (b) Delamination. (Not to scale)

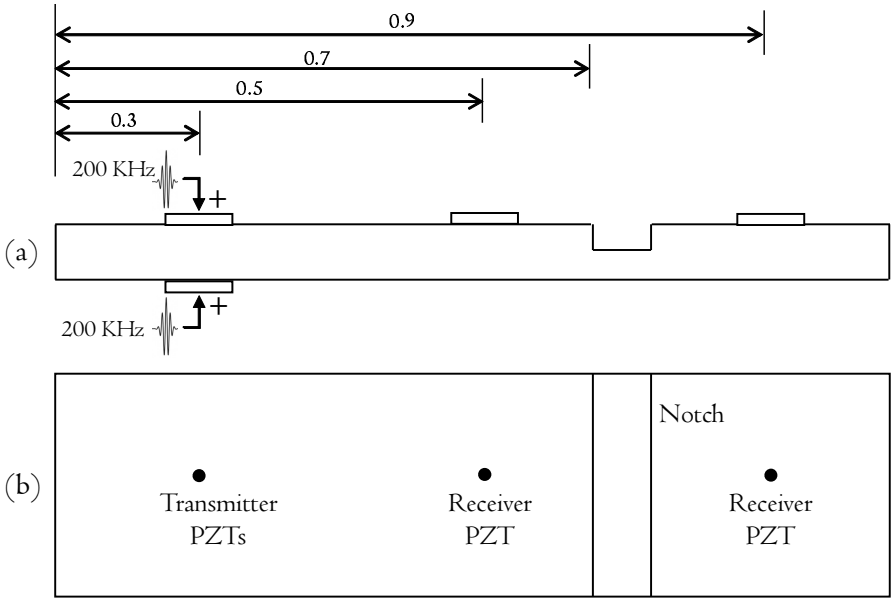

Figure 4: Schematic representation of the notched plate set-up: (a) front view; (b) plan view

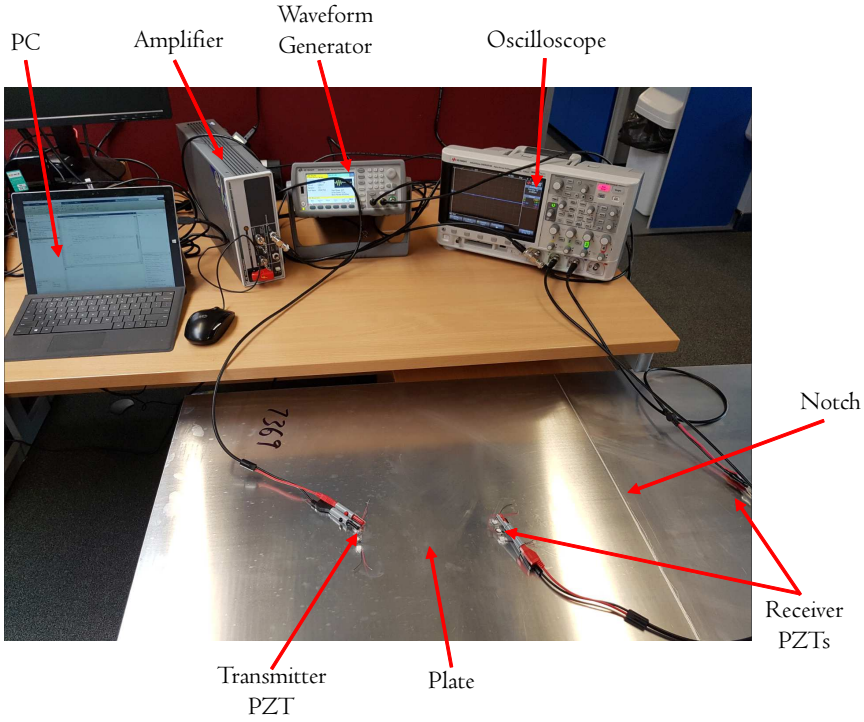

Figure 5: Assembly of the experimental configuration

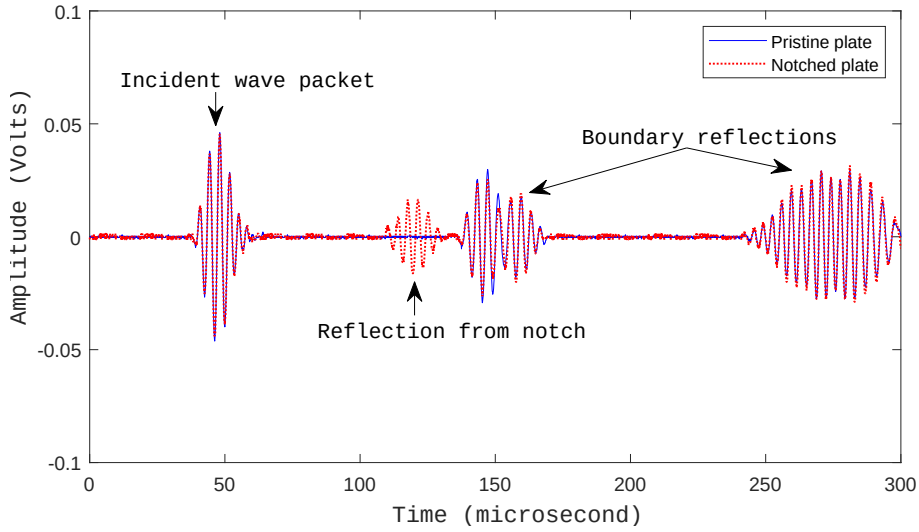

Figure 6: Superimposed experimental time record for pristine (-) and notched (. . .) plates. Notch is 1 mm deep and 5 mm wide

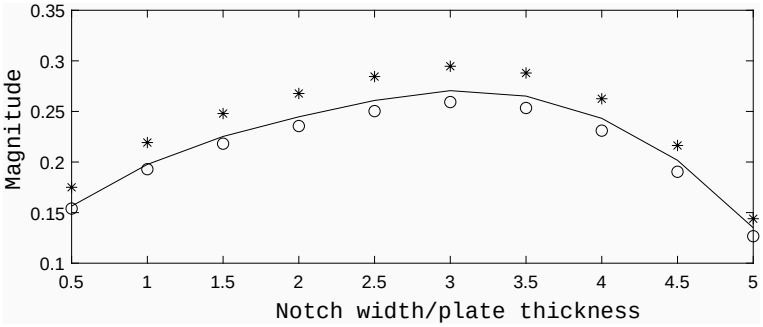

(a) 25% notch depth/plate thickness

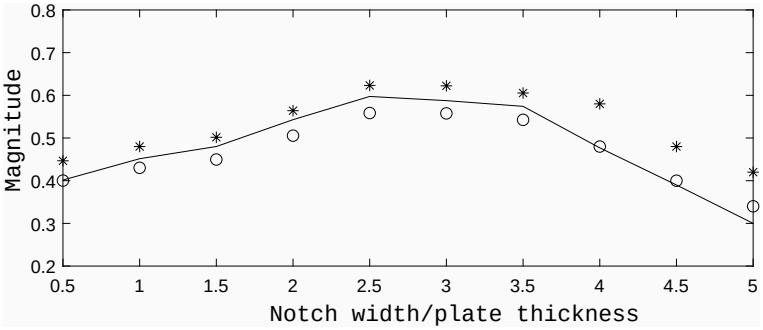

(b) 50% notch depth/plate thickness

Figure 7: Wave reflection coefficients from the notch as a function of the notch width/plate thickness: Current scheme (o), Experimental measurements (-), WFE-FE methodology [42] (*)

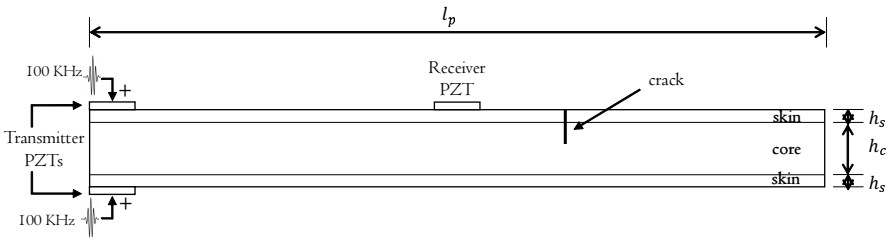

(a) Plate with crack

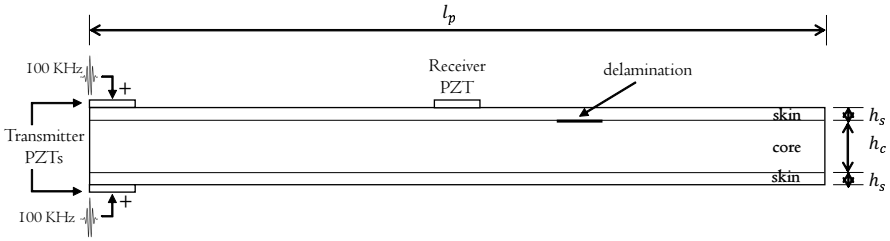

(b) Plate with delamination

Figure 8: Schematic of the FE calculation configuration for sandwich plates with (a) crack and (b) delamination

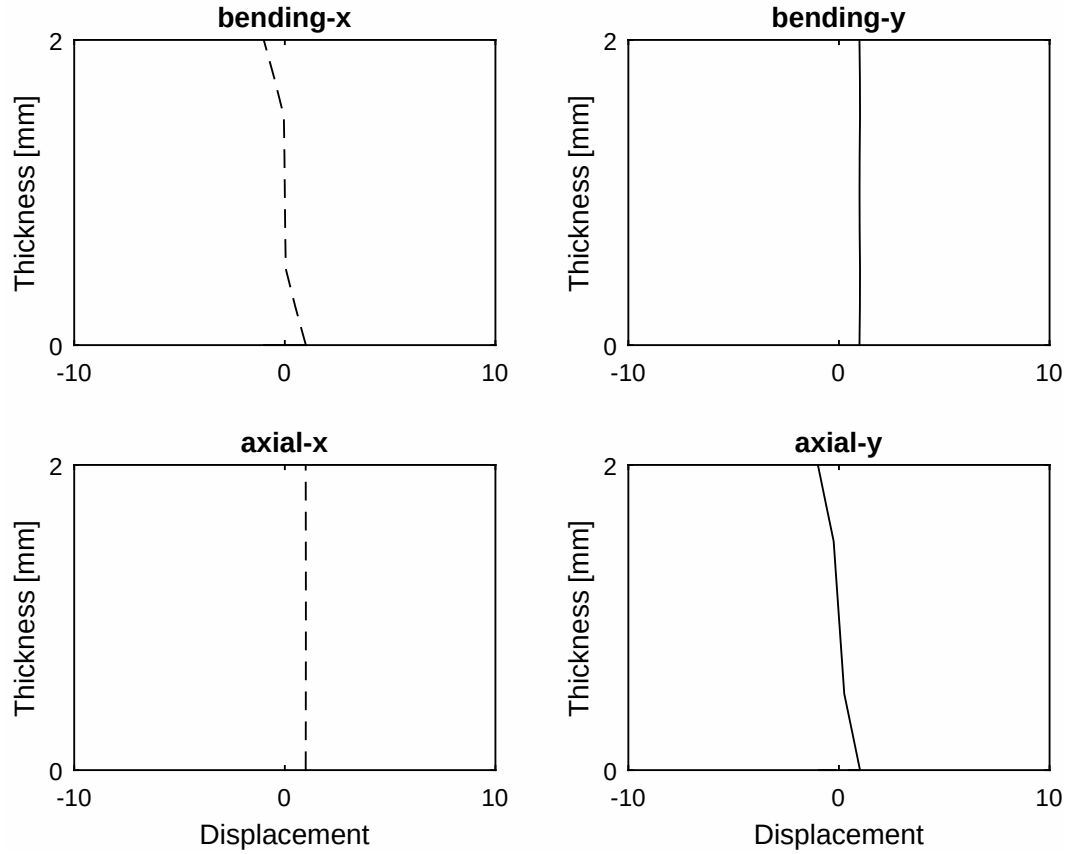

Figure 9: Mode shapes of the propagating waves in the sandwich plate at 100 kHz; left column: in-plane, right column: out-of-plane.

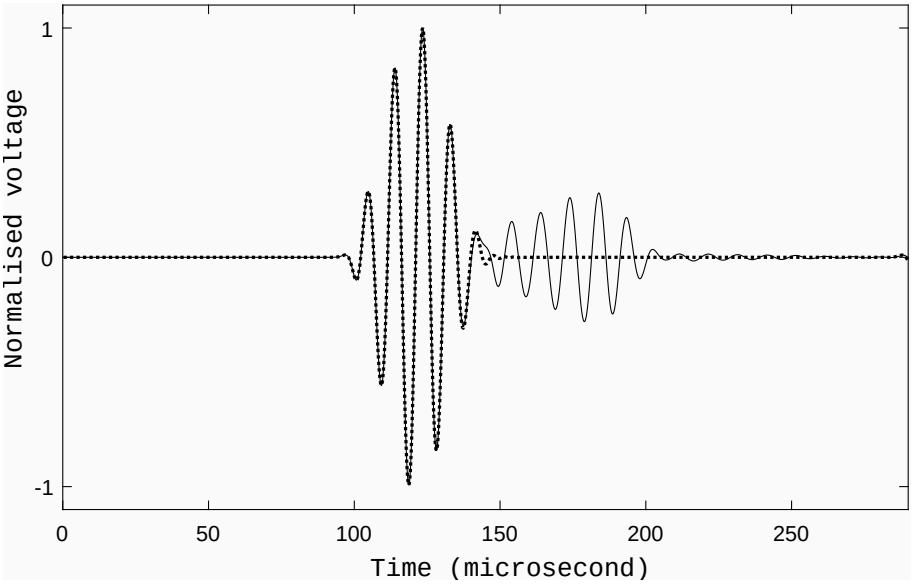

Figure 10: Superimposed time history predictions for the pristine plate ($\cdots$) and the plate with linear crack (-)

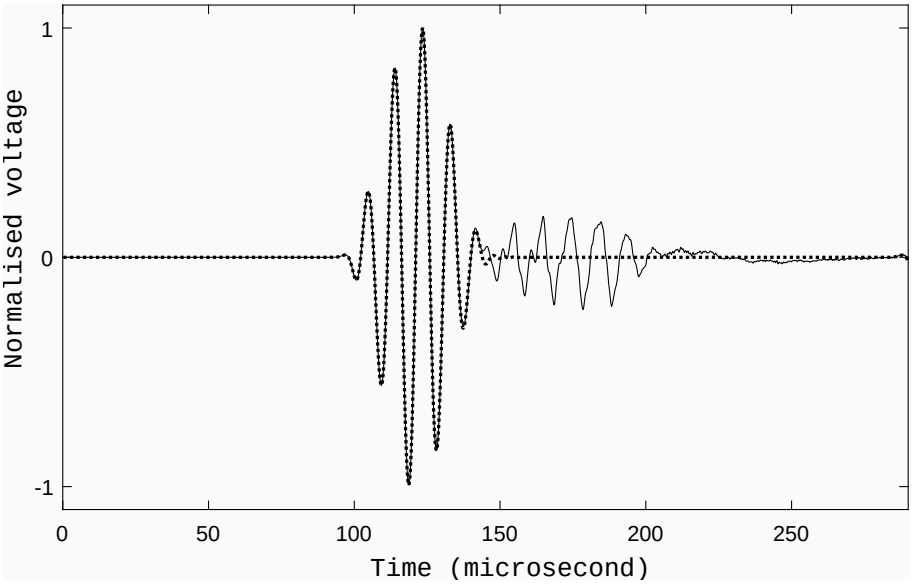

Figure 11: Superimposed time history predictions for the pristine plate (· · ·) and the plate with nonlinear crack (-)

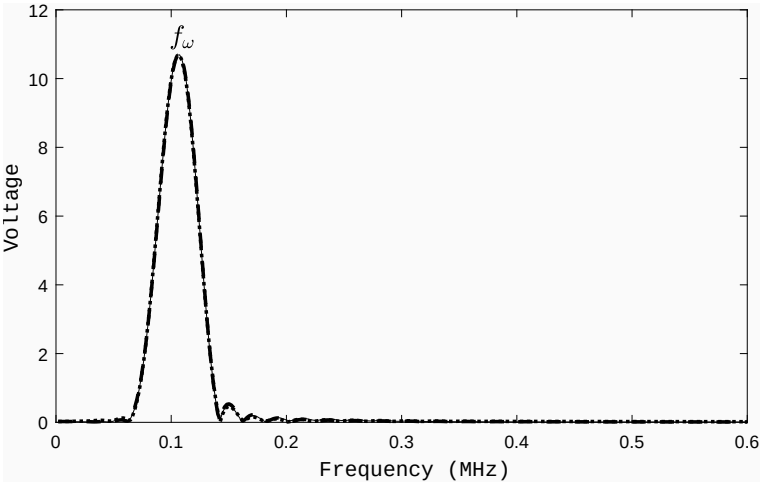

(a) Incident signal

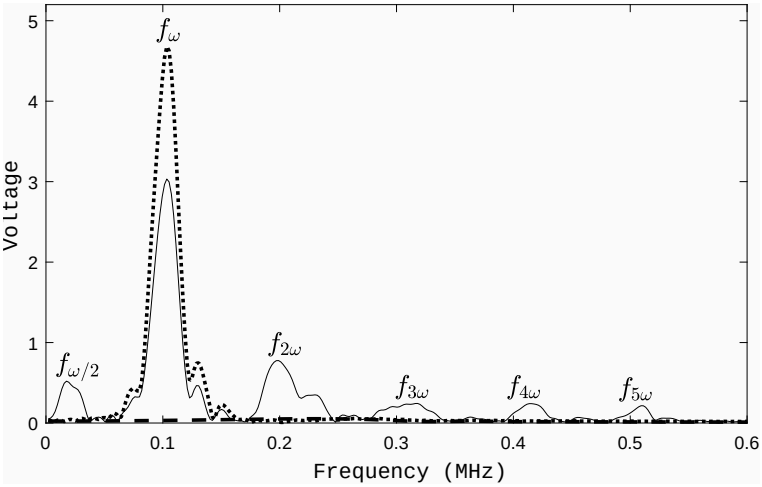

(b) Reflected signal

Figure 12: Superimposed frequency spectral of the incident and the reflected wavelets: pristine plate (- -); plate with linear crack ($\cdots$); plate with nonlinear crack (-)

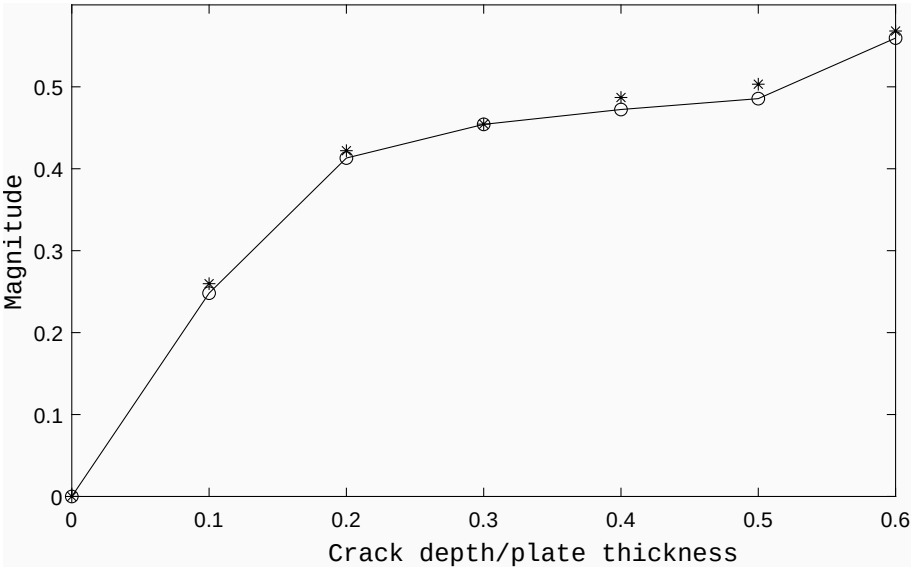

Figure 13: Wave interaction reflection coefficients for the plate with linear crack: present methodology (-o); computation as in [42] ($*$)

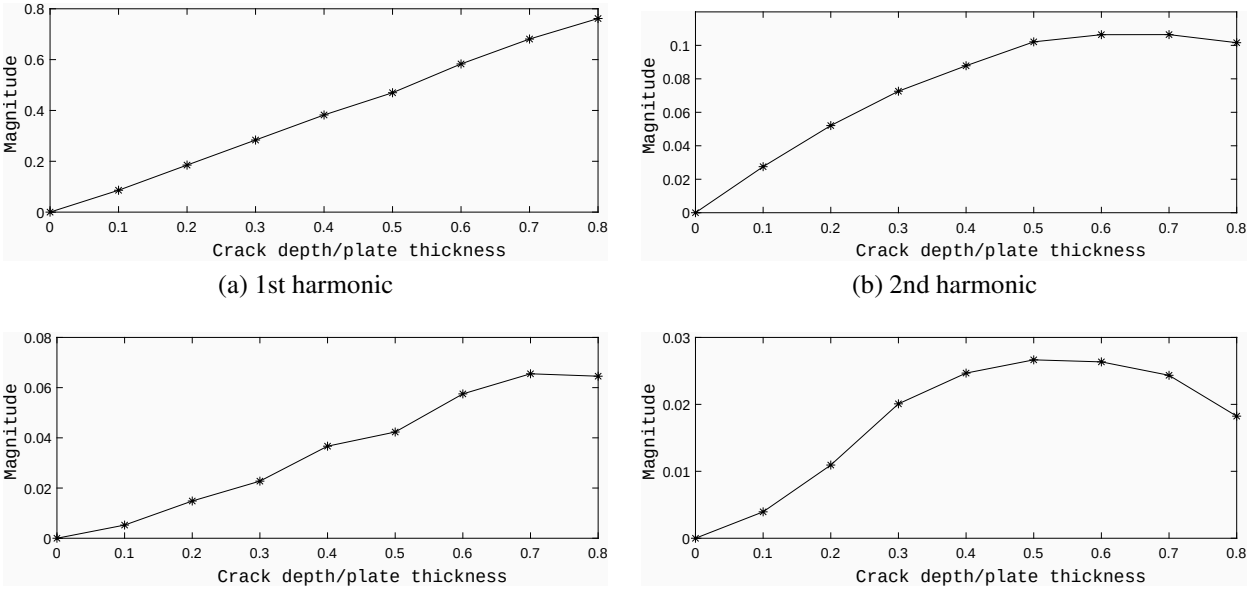

(a) 1st harmonic

(b) 2nd harmonic

(c) 3rd harmonic

(d) 4th harmonic

Figure 14: Wave interaction reflection coefficients for the plate with nonlinear crack at different harmonic frequencies

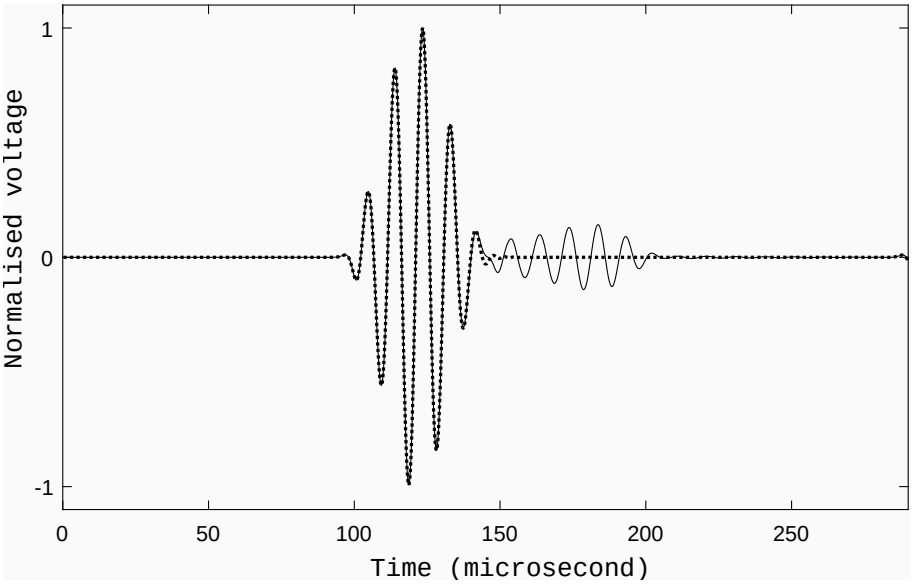

Figure 15: Superimposed time history predictions for the pristine plate ($\cdots$) and the plate with linear delamination (-)

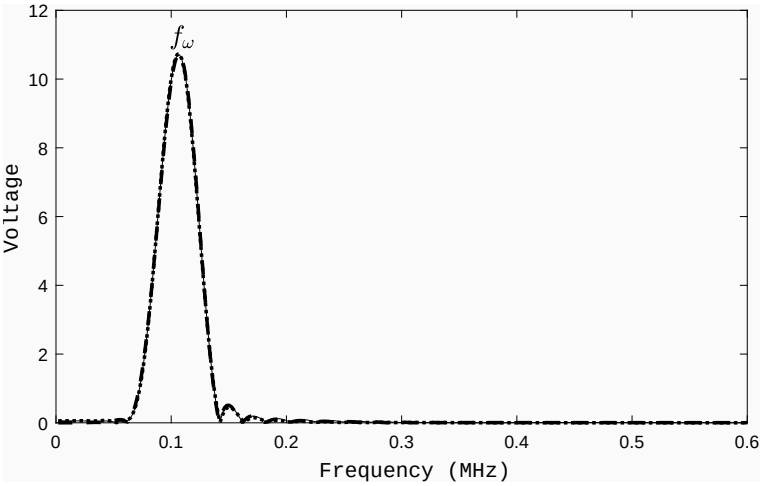

(a) Incident signal

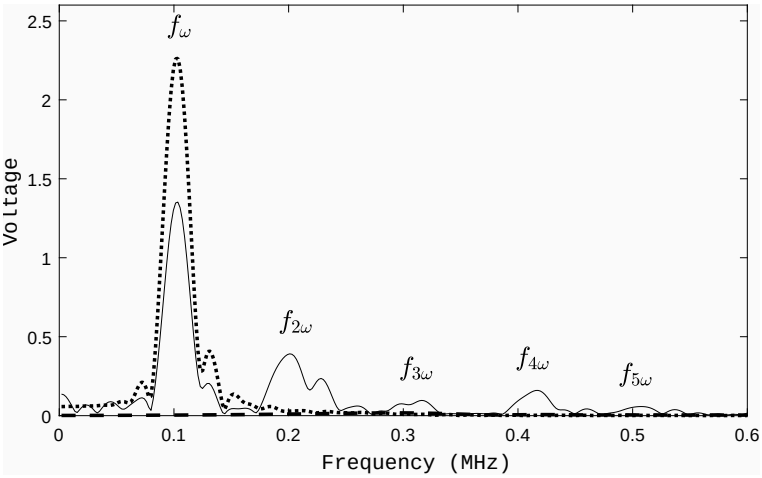

(b) Reflected signal

Figure 16: Superimposed frequency spectral of the incident and the reflected wavelets: pristine plate (- -); plate with linear delamination ($\cdots$); plate with nonlinear delamination (-)

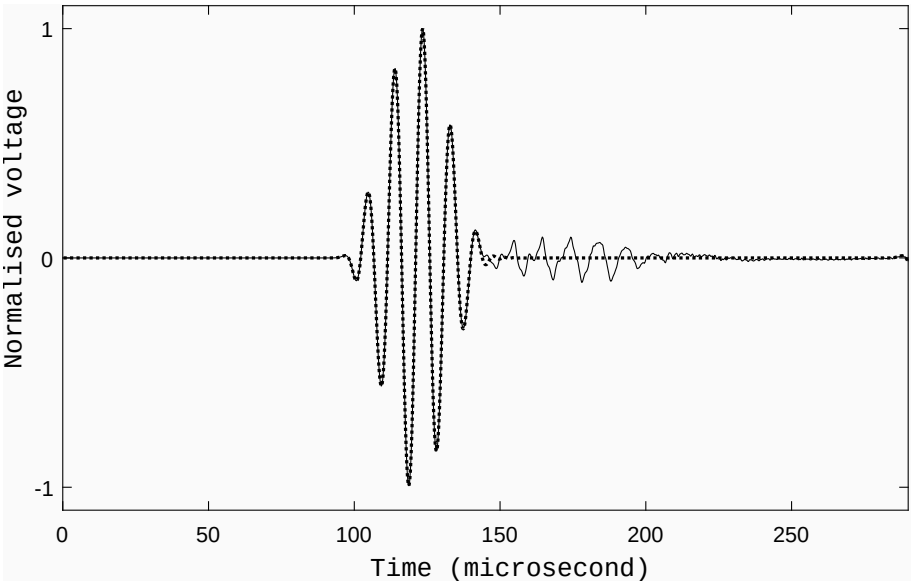

Figure 17: Superimposed time history predictions for the pristine plate ($\cdots$) and the plate with nonlinear delamination (-)

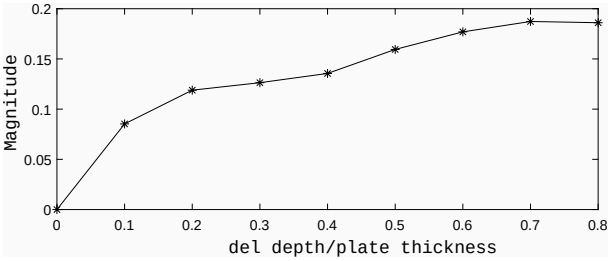

(a) 1st harmonic

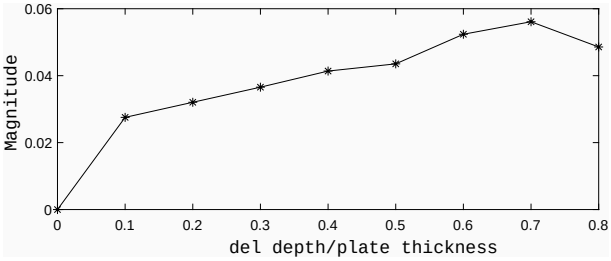

(b) 2nd harmonic

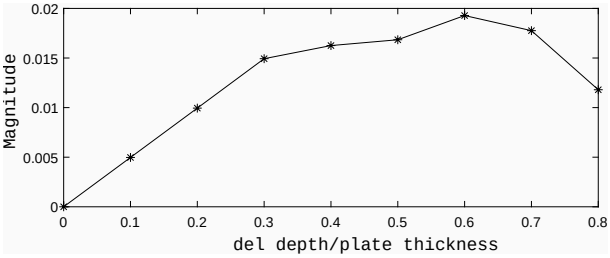

(c) 3rd harmonic

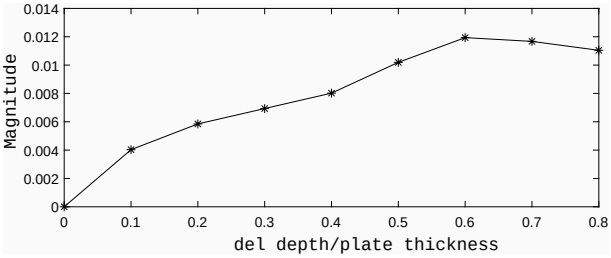

(d) 4th harmonic

Figure 18: Wave interaction reflection coefficients for the sandwich plate with nonlinear delamination at different harmonic frequencies